Supplement of Atmos. Chem. Phys., 26, 15445–15459, 2026
https://doi.org/10.5194/acp-26-15445-2026-supplement
© Author(s) 2026. CC BY 4.0 License.



Atmospheric Chemistry and Physics
Open Access
EGU

Supplement of

Springtime East Asian dust heating contributes to interannual poleward shift of the North Pacific storm track

Anbao Zhu et al.

Correspondence to: Xin Huang (xinhuang@nju.edu.cn)

The copyright of individual parts of the supplement might differ from the article licence.

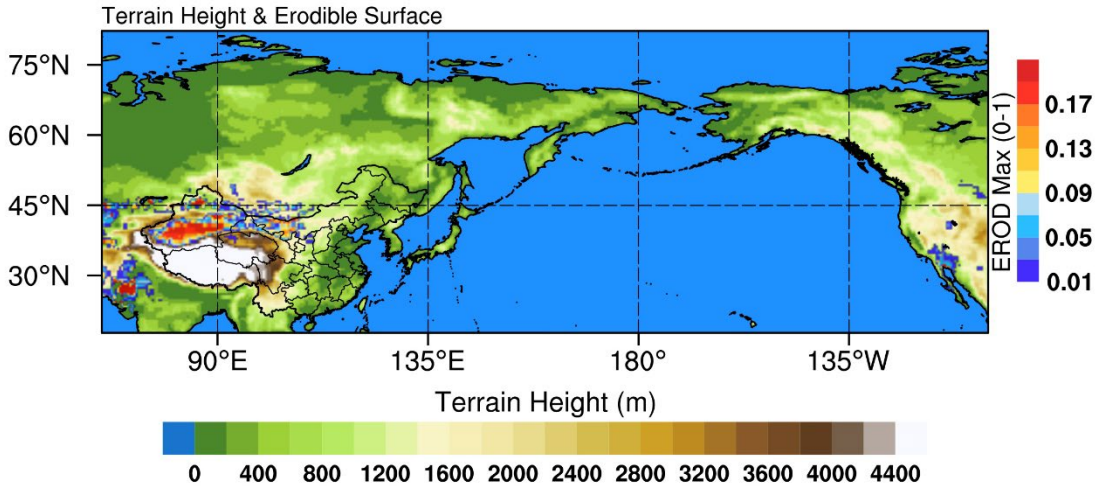


Figure S1. Model domain configuration showing terrain height (shading; m) and the fraction of erodible surface (EROD; dimensionless, 0–1) derived from the maximum across three soil types (sand, silt, and clay), which serves as the dust source function in the Shao (2004) dust emission scheme implemented in WRF-Chem.

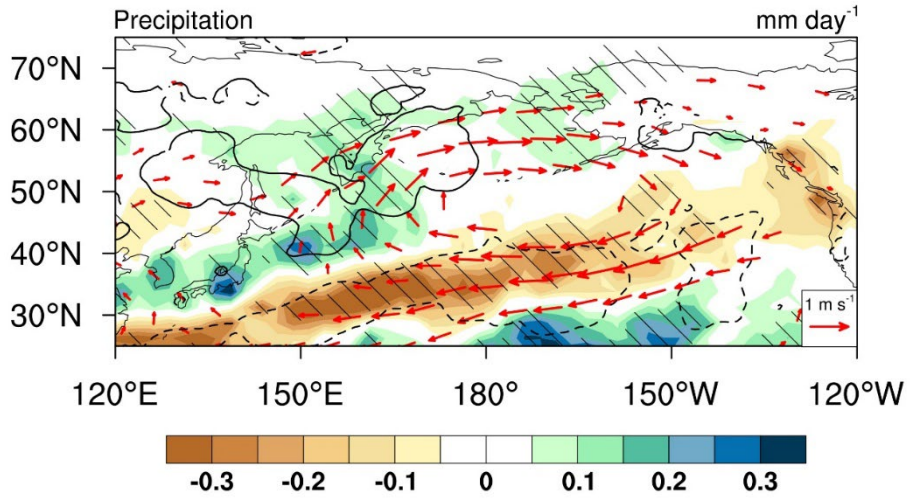


Figure S2. Regressions of anomalies in precipitation (shading; mm day^{-1}) and 850 hPa wind (vector; m s^{-1}) onto the standardized EADI_IA. Hatching and red vectors indicate that the regressed anomalies of precipitation and wind are statistically significant at the 95 % confidence level based on a Student's t test, respectively. Black contours denote the statistically significant regions of the regressed $V'T'_{850}$ anomalies shown in Figure 3b, with solid and dashed lines representing positive and negative values, respectively.

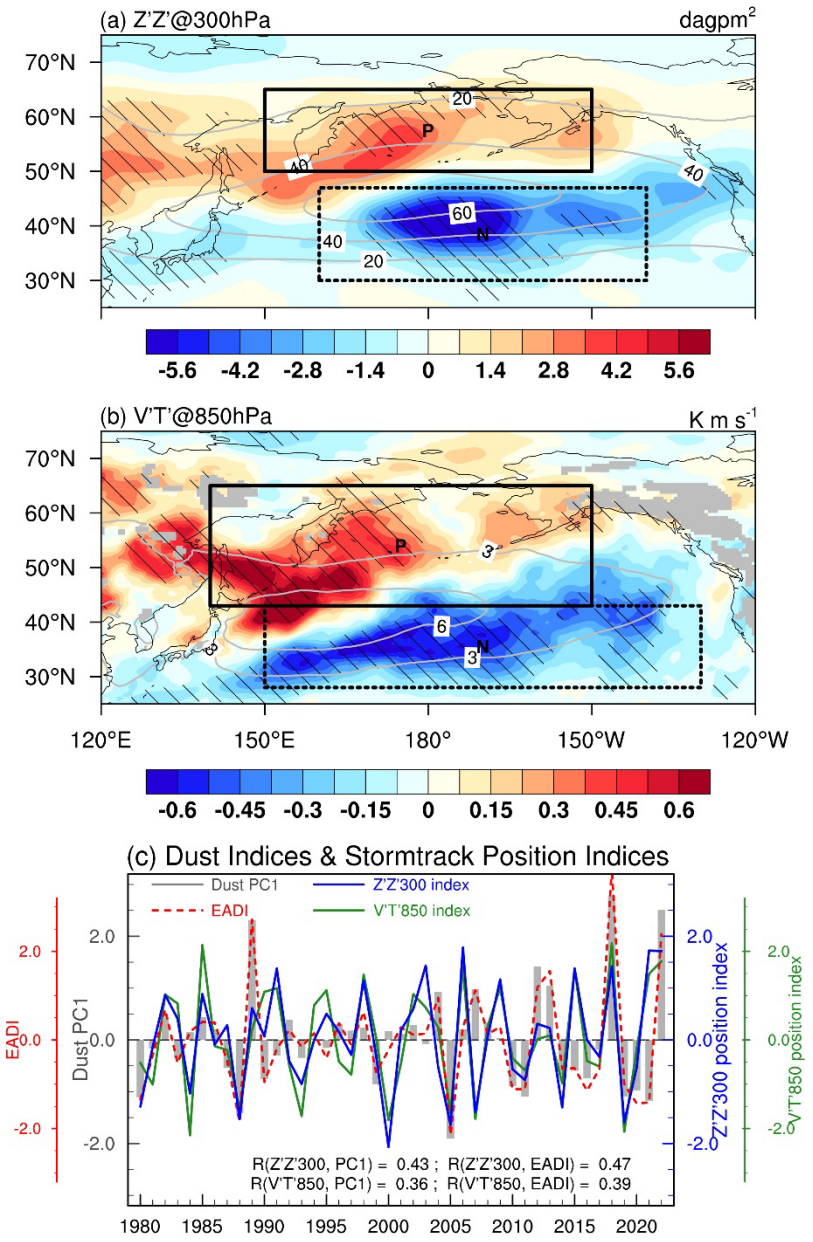
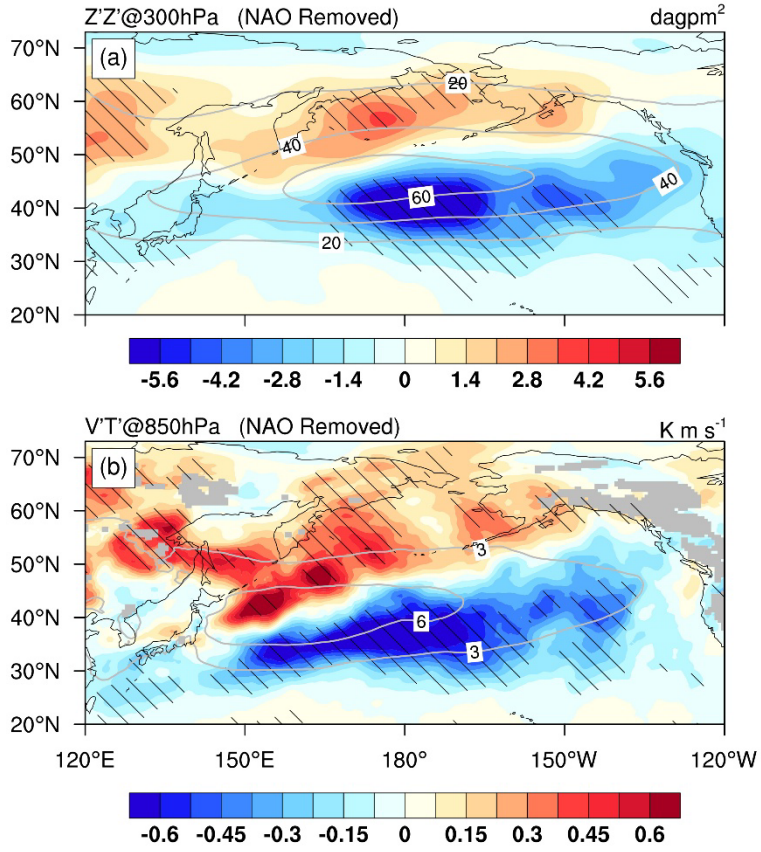


Figure S3. (a, b) Same as Figure 3, with the black solid (dashed) boxes denoting the northern (southern) regions used to define the storm track position indices. For (a) $Z'Z'_{300}$, the northern and southern boxes are 50°–65°N, 150°E–150°W and 30°–47°N, 160°E–140°W. For (b) $V'T'_{850}$, they are 43°–65°N, 140°E–150°W and 28°–43°N, 150°E–130°W. (c) Time series of the standardized interannual components of dust PC1 (grey bars), the EADI (red dashed line), and the $Z'Z'_{300}$ (blue line) and V'T'850 (green line) position indices during 1980–2022. Each position index is defined as the area-averaged value over the northern box minus that over the southern box. The correlation coefficients between the storm track position indices and the dust indices are shown in (c).



41

42 **Figure S4. Same as Figure 3, but with the concurrent spring (MAM) NAO signal linearly removed from all**
43 **variables before the regression. Grey contours denote the climatological spring mean of (a)** $Z'Z'_{300}$ **and (b)**
44 $V'T'_{850}$**. Hatching denotes the anomalies statistically significant at the 95% confidence level based on the**
45 **Student's t test.**

46

47

48

49

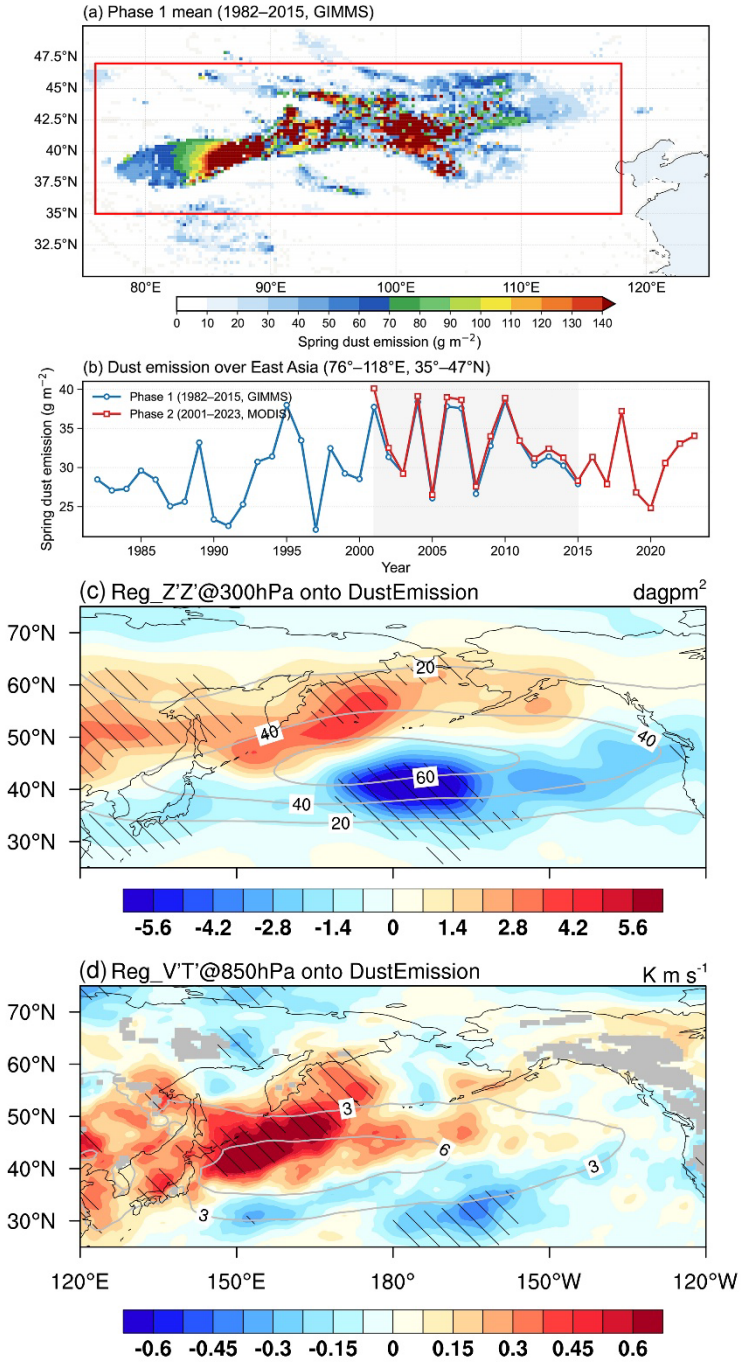


Figure S5. East Asian spring dust emission from Fu et al. (2026) and the associated storm-track anomalies. (a) Mean spring dust emission (g m^{-2}) for 1982–2015, derived from GIMMS vegetation data. The spatial distribution for 2001–2023 derived from MODIS data is similar and is not shown. The red box marks the EADI source region (35°–47° N, 76°–118° E). (b) Time series of spring dust emission averaged over the red box in (a). The blue line is based on GIMMS (1982–2015) and the red line on MODIS (2001–2023). Grey shading marks their overlap period (2001–2015). (c, d) Regressions of spring (MAM) (c) $Z'Z'_{300}$ (dagpm^2) and (d) $V'T'_{850}$ (K m s^{-1}) from MERRA-2 onto the standardized interannual component of the dust emission index for 1982–2022. The index is built from the GIMMS-based series for 1982–2000 and the MODIS-based

series for 2001–2022. Grey contours show the climatology. Hatching marks regions significant at the 95 % confidence level.

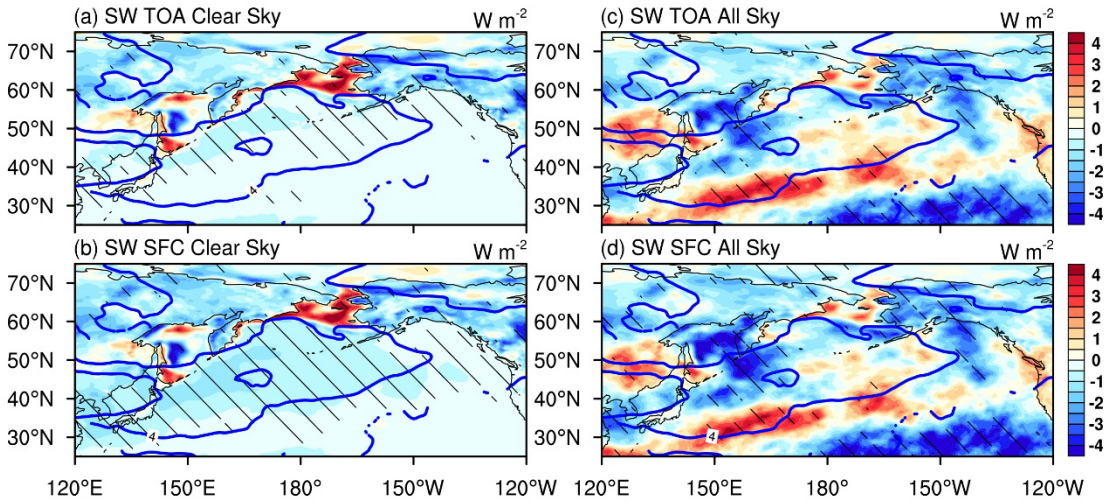


Figure S6. Regressions of anomalies in shortwave radiative fluxes (shading; W m^{-2}) at (a, c) the top of the atmosphere (TOA), and (b, d) at the surface (SFC) and dust column mass density (blue contour with interval of 2 mg m^{-2}) onto the standardized EADI_IA for (a, b) clear-sky conditions and (c, d) all-sky conditions. The regressed fields therefore give the response per one standard deviation of EADI_IA. Positive values denote an increase in net downward SW flux. Hatching indicates that the regressed anomalies in shortwave radiative fluxes are statistically significant at the 95 % confidence level based on a Student's t test. The all-sky minus clear-sky differences mainly reflect the cloud redistribution associated with the storm track shift.

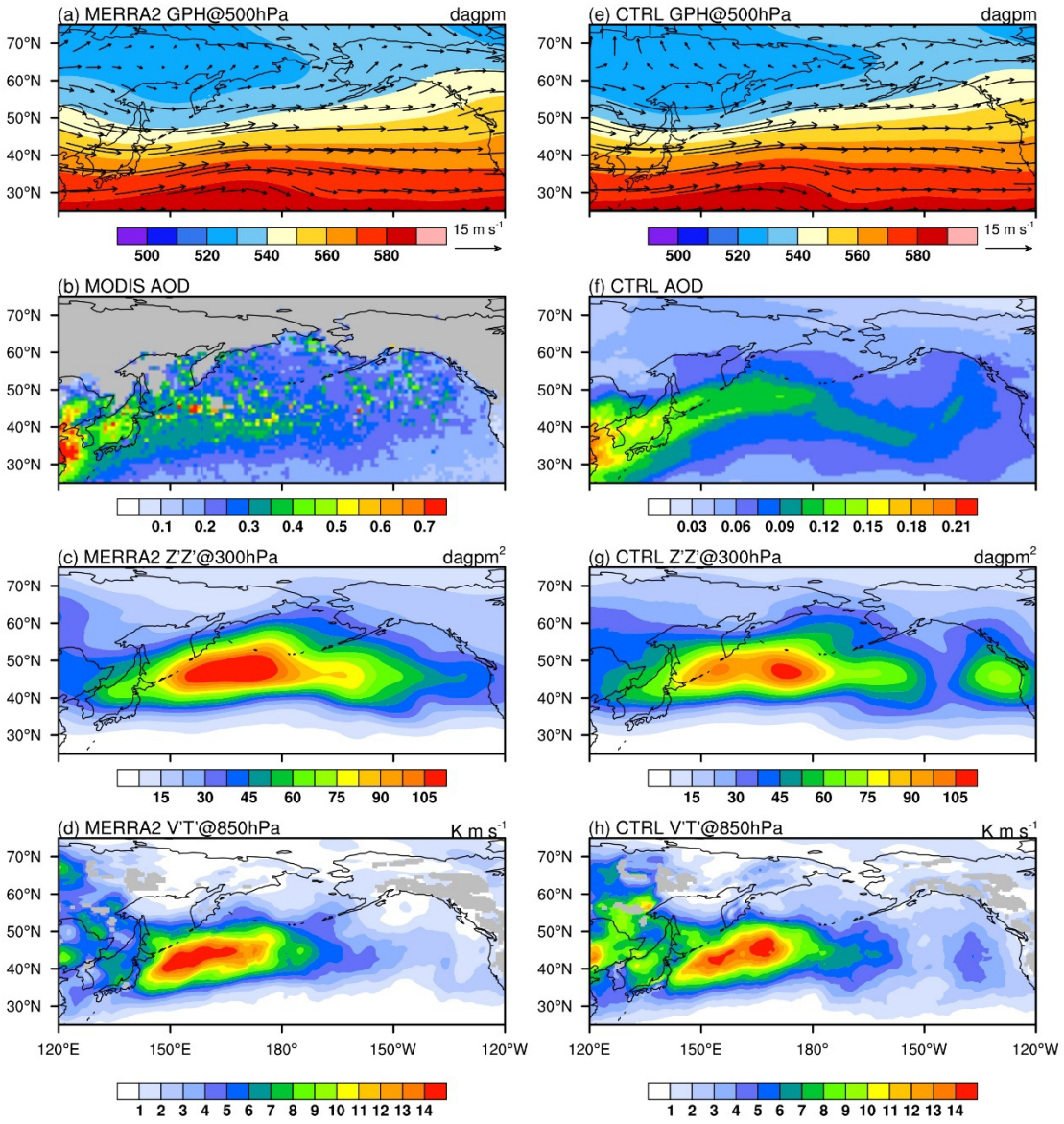


Figure S7. Spatial distributions of (a, e) 500 hPa geopotential height (shading; dagpm) and wind (vectors; m s^{-1}), (b, f) aerosol optical depth (AOD; shading; unitless), (c, g) $Z'Z'_{300}$ (shading; dagpm2), and (d, h) $V'T'_{850}$ (shading; K m s^{-1}) averaged over spring (MAM) of 2018. The left column (a, b, c, d) represents the observational and reanalysis data (MERRA-2 for meteorological fields and MODIS for AOD). The right column (e, f, g, h) shows the corresponding ensemble mean of the WRF-Chem CTRL experiment.

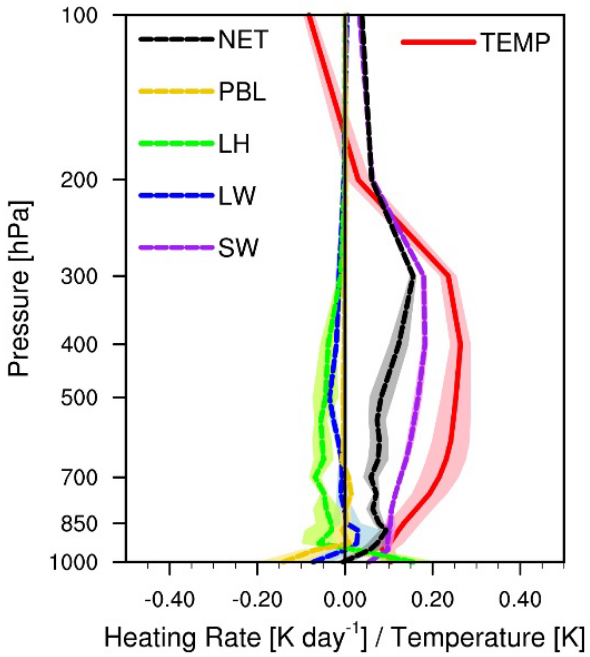


Figure S8. Vertical profiles of differences (CTRL minus NoDust) in temperature (solid red line; K) and atmospheric heating rates (dashed line; K d^{-1}) averaged over the North Pacific (150°E–150°W, 35–53°N, as outlined in Figure 7c). Here, atmospheric heating rates include shortwave (SW) and longwave (LW) radiation heating, latent heating (LH, i.e., heating from the microphysics and cumulus scheme), and heating from the planetary boundary layer (PBL) scheme. Net heating rate (NET) = SW + LW + LH + PBL.

References:

Fu, Y., Wu, C., Gao, S., Peñuelas, J., Camarero, J. J., Zhang, J., Li, D., Zheng, X., Li, Z., Wang, Y., Liang, E., and Piao, S.: Vegetation greening drives long-term dust mitigation in Eastern Asia, Nature Communications, 17, 1729, 10.1038/s41467-026-68427-y, 2026.

Shao, Y.: Simplification of a dust emission scheme and comparison with data, J. Geophys. Res.-Atmos., 109, D10202, https://doi.org/10.1029/2003JD004372, 2004.